Forschung im Ingenieurwesen (2025)89:33
https://doi.org/10.1007/s10010-025-00816-z

ORIGINALARBEITEN/ORIGINALS

Validation of models for calculating the NVH behavior of gearbox systems in an elastic multibody simulation

Stefan Wischmann[1] · Alexander Mann[2] · Georg Jacobs[1] · Christian Brecher[2] · Gregor Hoepfner[1] · Christian Westphal[2]

Received: 17 September 2024 / Accepted: 12 February 2025
© The Author(s) 2025

Abstract

The acoustic behavior of technical products—referred to as Noise, Vibration, and Harshness (NVH)—forms an important criterion in customers' purchasing decisions, e.g. in the automotive sector. Thus, optimizing the NVH behavior is essential during product development. NVH is influenced by dynamic excitations and the transfer of sound from the location of excitation to a receiver such as the driver. As the electrification of the mobility sector increases, gear mesh excitations contribute significantly to the noise of a vehicle, which was previously dominated by the combustion engine. The time-varying stiffness of the gear mesh is the main excitation in drivetrains and therefore needs to be optimized during product development. Elastic multi-body simulation (eMBS) has become an established method for modeling NVH characteristics of drivetrains. In order to evaluate the effect of gear mesh designs on a drivetrain's excitations and therefore its NVH behavior, the time-varying stiffness of the gear mesh has to be incorporated into eMBS models. Today, this is either done by applying quasi-static transmission errors onto a model in frequency domain thereby neglecting the influence of the system's oscillations back on the gear mesh excitations, e.g. by axial misalignment of the meshing shafts. Alternatively, analytical stiffness calculations are included in eMBS models in time-domain. However, these approaches are not yet validated. Also, incorporating the interaction between a flexible gear wheel and the gear mesh stiffness is paramount for NVH models of gears. Within previous works, a method for incorporating externally calculated gear mesh stiffnesses into eMBS has been proposed to overcome these challenges. The goal of this paper is to compare, validate and enhance the existing eMBS modeling methods of gear mesh stiffnesses with respect to their ability to model the dynamic behavior of gear boxes, defined by natural frequencies and critical operating points. A two-step approach consisting of quasi-static and dynamic validations is conducted. An improvement in accuracy between simulation and measurement of 10 dB is achieved compared to analytical eMBS methods.

1 Introduction

In the context of shortening product life cycles, virtual product development (VPD) methods enable reducing the number of physical prototypes. This can save development costs and reduce development times. Numerical models are essential as a VPD tool in order to cope with increasing demands for product individualization. At the same time, customers are increasingly focusing on the acoustic properties and comfort behavior of products, which are summarized under the term NVH (noise, vibration, harshness) [1, 2].

In the automotive market in particular, NVH behavior is often one decisive factor in purchasing behavior. The emitted noise is a function of the excitation in combination with the transfer path. With the increasing electrification of passenger vehicles and the consequential loss of the low-frequent, broadband noise of internal combustion engines, which previously dominated the NVH of passenger cars and masked high-frequent tonal noises, gear excitation due to periodically changing mesh stiffness and manufacturing deviations is one of the dominant excitation mechanisms. The design of flexible gear bodies to exploit the lightweight design potential creates a challenge, as the elasticity of the gear bodies interacts with the tooth mesh stiffness. In or-

✉ Stefan Wischmann
stefan.wischmann@imse.rwth-aachen.de

[1] Institute for Machine Elements and Systems Engineering, RWTH Aachen University, Schinkelstr. 10, 52062 Aachen, Germany

[2] Laboratory for Machine Tools and Production Engineering (WZL), RWTH Aachen University, Steinbachstraße 19, 52074 Aachen, Germany

Published online: 25 February 2025

der to identify possible problems in NVH behavior at an early stage of the development process and derive optimization measures, the methods of elastic multi-body simulation (eMBS) have become established in the context of VPD. Therefore, gear mesh excitations have to be considered in eMBS models to allow for a model-based optimization of drivetrains' dynamic behaviors during the development process.

The state of the art provides various approaches for calculating time-varying tooth pair stiffnesses and consider them in eMBS models and which are available in commercial software such as SIMPACK or MASTA and which consider the gear mesh stiffness either by analytical equations or FE calculations. A detailed validation of this method considering both the quasi-static tooth mesh stiffness and the structural dynamic excitation behavior in eMBS is still pending. The aim of this study is therefore to validate the methods in a two-step process. In the first step, the tooth strain is to be investigated under static load using a pulsator test rig in order to separate the gear tooth area from the gear body. As a second step, test rig investigations on the gear system under static and dynamic operating conditions provide information on the excitation behavior. Therefore, the development engineer will be provided with a validated methodology that enables reliable predictions even when taking into consideration time-varying stiffnesses.

First, in Sect. 2, an overview over the state of the art of eMBS models for calculating the NVH behavior of drivetrains as well as an introduction to calculating a gear mesh stiffness is presented. Section 3 specify the deficit in the state of the art addressed in this work and Sect. 4 describes the corresponding approach. Section 5 specifies the case-study, describes and discusses the results and validates the models. A conclusion and outlook is given in Sect. 6.

2 State of the art

To understand the requirements for a validated model of gear mesh excitations within NVH simulation models, in what follows, an overview over existing methods for calculating the time-varying gear mesh stiffness as well as an introduction into NVH system simulation models is given.

2.1 NVH system simulation models

Modeling the NVH properties of drivetrains requires models of the excitation mechanisms, the transfer behavior from the source of excitation to the receiver and models of the acoustic radiation and perception [3–5]. An exemplary model of an electromechanical drivetrain is visualized in Fig. 1. It consists of models for the gear mesh excitations and the electromagnetic excitations (visualized in orange) as well as models for the stiffness and damping of roller bearings, elastomeric mounts, flexible bodies and dynamics in bolted joints (visualized in blue). While the excitation mechanisms apply dynamic, time-varying loads to the system, thereby causing vibration and subsequently audible noise, the transmitting elements (visualized in blue) influence the stiffness and damping of the systems, which influences eigen frequency and the transmission characteristics from the source of the excitation to the sound

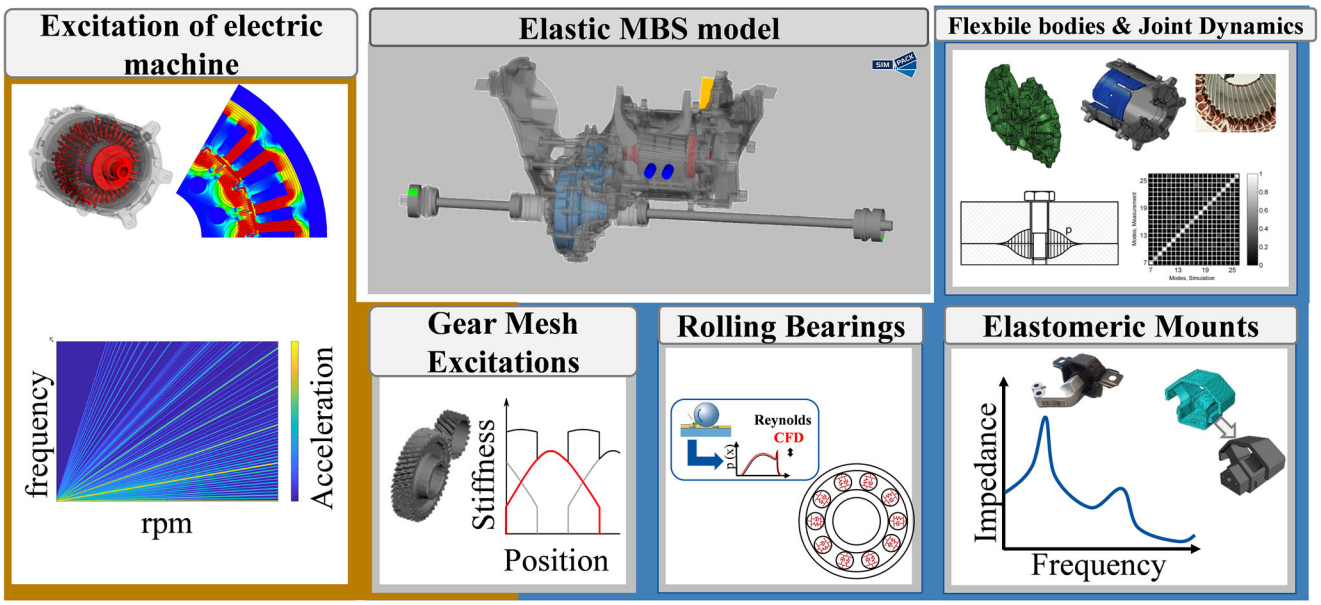


Fig. 1 Modeling elements in an exemplary NVH system simulation model according to [8]. Orange: Excitation mechanisms, blue: Transfer behavior

radiating surfaces, amplifying or decreasing the magnitude of oscillations caused by the excitation mechanisms. Many of these effects are nonlinear. For example, the gear mesh and bearing stiffness depend on the transmitted load [6, 7]. Also, the stiffness and damping of the elastomeric components as well as bolted joints depend on preload, vibration amplitude and frequency [8, 9]. Furthermore, the excitation and the transfer models are interacting with each other. For example, an eccentricity, induced by bearing clearance, can modulate electromagnetic forces and gear mesh forces, altering the excitation behavior [10]. To capture such nonlinear interactions, modeling the NVH behavior of drive trains must be done in time-domain [3]. However, these time-domain analyses are computationally expensive compared to time-invariant analyses. Therefore, to increase computational efficiency, NVH system simulation models are often implemented in an elastic multi body simulation environment based on modal reduction [11]. By reducing the degrees of freedom of flexible bodies through modal reduction, significant improvements in computational efficiency are achieved.

Therefore, models of gear mesh excitations which can be used in NVH System simulation models have to fulfill the following requirements:

- Implementation in an eMBS environment
- Suitable for time-domain analysis
- Capability of applying forces on modally reduced bodies of flexible components

2.2 Calculation of gear mesh stiffness

In what follows, the underlying excitation mechanism in gear stages is described. Models for calculating the gear mesh stiffness are presented with respect to fulfilling the requirements derived from the state of the art of NVH system simulation models in Sect. 2.1.

The contact areas of two gears are not ideally rigid due to HERTZIAN pressures and the bending flexibility of the teeth, but have a finite contact stiffness that varies over the meshing [12, 13]. The tooth meshing stiffness is influenced by material properties, geometry parameters and dynamic loads. A typical overall gear mesh stiffness of a cylindrical gear pair is shown as a function of the line of action in Fig. 2.

One method for modeling gear excitations is to initially calculating the total gear stiffness and then importing it into the simulation model. The gear contact stiffnesses are usually calculated based on characteristic maps. The contact stiffnesses are stored as a function of the rolling path and the load. An angle-dependent characterization is also possible. This use of characteristic maps is known as "external stiffness" and is regarded as resource-efficient as it eliminates the need to perform a complex calculation of gear stiffness for each individual time step of a simulation [15–17].

In order to implement this modeling approach in an eMBS environment, force elements were developed that are capable of applying gear forces to flexible bodies within an elastic multi-body simulation [15, 18–20]. Complex models allow implementing the non-linear gear stiffness as a function of several input variables.

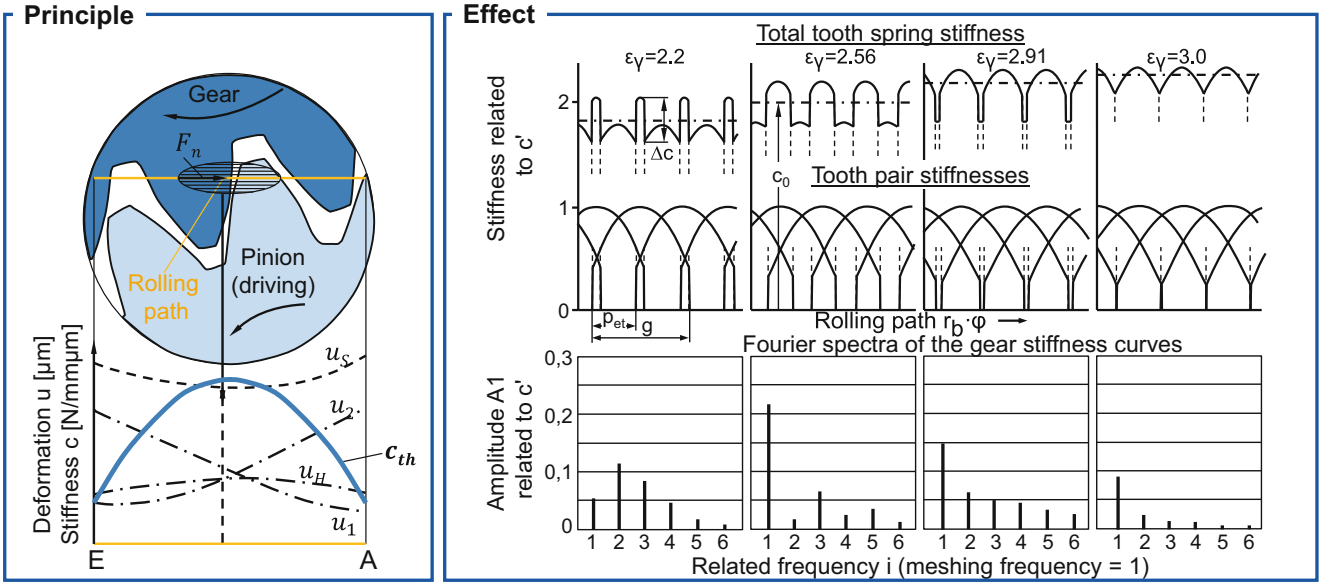


Fig. 2 Tooth pair stiffness with respect to the line of contact according to MÖLLERS [12, 14]

Methods to calculate the total gear stiffness can be classified as analytical [21, 22], numerical [18, 23–25] or experimental [26, 27]. Analytical methods are based on simplified assumptions and mathematical models, while numerical methods often use finite element analysis (FEA).

A common approach is to use a single parallel spring-damper element along the line of action between the gears to model the contact during the meshing process. This approach is especially used for torsional vibrations. The advantage of this approach is the simplicity of the system and the resulting good computing efficiency. A disadvantage is the limited accuracy, particularly with high loads or deformations and manufacturing deviations [28–32].

Another approach divides the gear into a gear body and gear teeth models and connects them via spring-damper elements [16, 17, 33]. Different force application points for single and multiple meshes are considered. For higher levels of detail, the flexibility of individual teeth can be modeled using the finite element method [18, 34]. In this case, the load is distributed to several force application points along the pitch circle [35]. This method allows precise calculations in eMBS, as it considers the effect of a force application in the correct position. However, it requires considerable computing resources initially.

An analytical approach for calculating the tooth pair stiffness exists according to WEBER/BANASCHEK. It combines the elastic deformations due to bending, shear and tilting of a tooth under load to an overall stiffness based on the geometry and material properties of the tooth flanks [21].

The calculation of tooth stiffness according to ISO 6336 is available as a standardized basis [36]. The standard provides formulas for calculating the average spring stiffness of a tooth. These are based on material properties such as Young's modulus and Poisson's ratio as well as geometric parameters such as normal modulus, number of teeth and pressure angle. The ISO approach contains specific correction factors for influences such as multiple tooth meshes or dynamic effects, which makes it more comprehensive than the purely analytical approach of WEBER/BANASCHEK [37].

In conclusion, various methods for calculating gear mesh stiffness in elastic multibody simulations were presented, including analytical approaches such as WEBER/BANASCHEK and ISO 6336, numerical methods with finite element analyses and simplified and extended spring-damper models; the choice of method influences the balance between calculation accuracy and computational cost. However, only a few of these methods are implemented in eMBS models and are therefore suitable for NVH system simulation. One widely used, commercially available implementation is provided by the eMBS software SIMPACK, which allows the user to choose between an ISO approach and a load-dependent WEBER/BANASCHEK approach for calculating the gear mesh stiffness [37]. The implementation allows the user to discretize the gear mesh stiffness along the axial direction in several slices to consider angular misalignments and the effect of micro geometries on the load distribution. It offers a choice between two possibilities to model the influence between gear mesh stiffness and flexible gear bodies: Method A applies tooth forces on the tooth root diameter at modally reduced degrees of freedom. Method B applies the tooth forces on the pitch diameter, calculating the influence of tooth bending from modally reduced FE bodies instead of ISO or WEBER/BANASCHEK and retains only the part of the HERTZ'ian contact stiffness in the ISO and WEBER/BANASCHEK approaches. While the approach is widely used, no thorough validation against experiment is publicly available [15].

The lack of validated eMBS implementations of gear mesh excitations has led to the development of the approach based on numerically pre-calculated arrays. For this reason, a method (VAMOS—VERZAHNUNGSMODELLIERUNG FÜR DIE SYSTEMSIMULATION) has been developed that enables the gear excitations to be taken into account in the eMBS in a computationally efficient way and at correct positions on the basis of a precalculation of stiffness maps. According to the VAMOS method, stiffness maps are calculated for parts of the gear body in which the strains are influenced by the tooth bending. This part of the gear is modeled separately from the gear body, of which the flexibility is considered using modal reduction [38]. The diameter, at which the tooth is separated from the gear body is called energy diameter, see Fig. 3 [38]. The fundamental approach of splitting gears into a flexible part and a tooth ring at a specific diameter and subsequently calculating gear

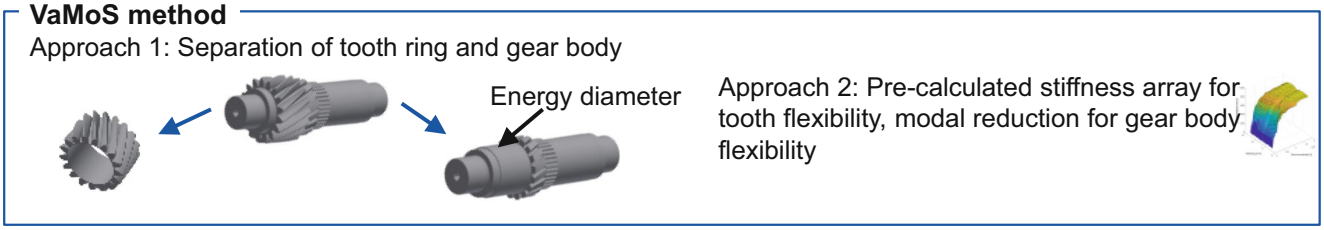


Fig. 3 VaMoS method: Splitting gears into tooth ring and flexible bodies according to [38], subsequent application of characteristic force maps

mesh stiffnesses only based on the tooth ring has already been published in [38]. The energy diameter is calculated based on the strain energy distribution in quasi-static loading. Specifically, the energy diameter is the diameter at which the strain energy density of a gear wheel which is subjected to a quasi-static load at the operating pitch diameter along the line of action decreases below 5% of the maximum strain energy density [38]. The evaluation of applying pre-calculated stiffness arrays in eMBS is discussed within this publication.

The VAMOS approach considers a pre-calculated gear mesh stiffness in the calculation chain [6]. However, it has not been validated in the eMBS [38–40]. Nevertheless, previous verifications have shown deviations, particularly in the dynamic behavior with regard to load-dependent natural frequencies. A detailed validation of methods considering both the quasi-static tooth mesh stiffness and the structural dynamic excitation behavior is still pending.

3 Problem formulation

While various methods for simulating gear mesh force excitations are available, there is a lack of systematic validation for high-fidelity time-domain models in eMBS simulations. Although individual models are verified to different extents against other simulation models, it is today unclear, which model is suitable for applying gear mesh excitations in time-domain in NVH system simulation models. It is especially unclear, how different scopes of NVH models influence the choice of suitable gear mesh excitation models. Possible scopes of dynamic models are as follows:

- Calculating the resonance frequency of a gear stage under different loads
- Calculating the influence of different gear body designs on the resonance frequencies
- Calculating the gear mesh excitation of the first gear mesh frequency as a rough approximation for the most dominant excitation order
- Calculating multiple higher harmonics of gear mesh excitations for a correct frequency spectrum of the calculated noise

Therefore, the goal of this contribution is to develop a validation method, which allows to quantify the aforementioned influences and to subsequently use the validation method to compare high-fidelity, time-domain NVH models of gear mesh excitations.

4 Approach

The proposed approach for validating and comparing different eMBS models of gear mesh excitations is visualized in Fig. 4 and consists of a static and a dynamic validation.

The aim of this first step is to provide an experimental case-study which allows for studying the influence of load and gear body design on resonance frequencies and excitation behavior both experimentally and numerically. In order to study the influence of different flexibilities of gear bodies during operational measurements, three different gear body designs (solid body, C body and I body) are designed and manufactured. This will enable an analysis of the interaction between gear body flexibility and gear mesh excitation as well as a comparison between different eMBS modeling methods with respect to their capability of capturing these effects. Secondly, eMBS models of the gear stage are created. This includes the generation of FE models used for modal reduction of the shafts and housing during eMBS

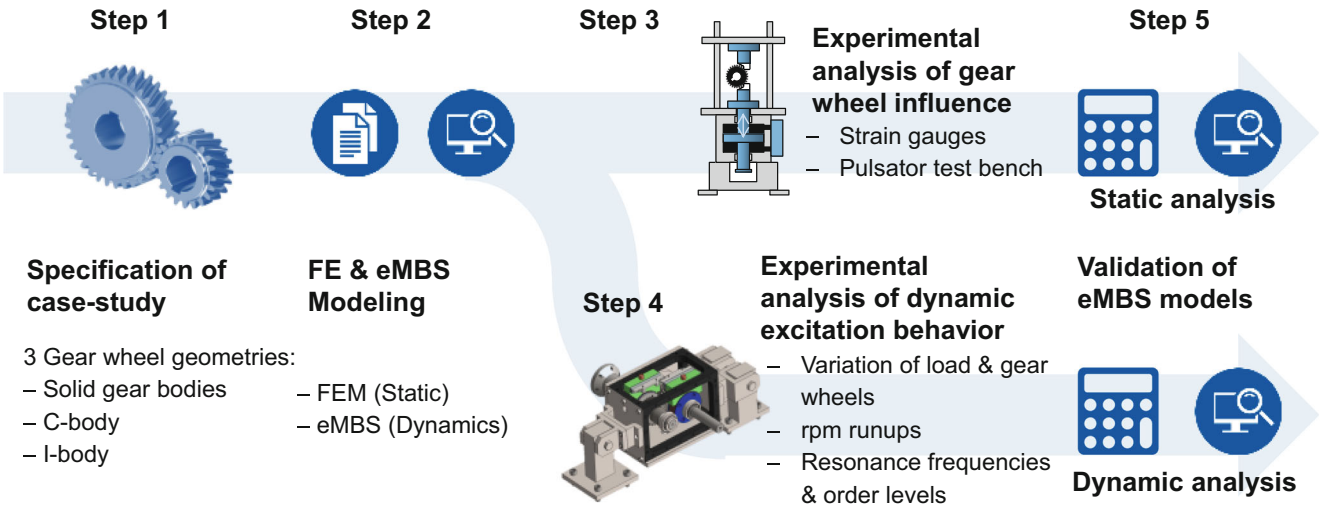


Fig. 4 Solution Approach

model generation. Models will be created both using the approach of separating tooth stiffness and gear body stiffness at the energy diameter [38] as well as the commercially available implementations in the eMBS software SIMPACK, Method A and B, see Chap. 2.2. Both methods rely on the calculation of gear mesh stiffnesses according to WEBER-BANASCHEK [41]. The eMBS models will be used subsequently for both the quasi-static as well as the dynamic validation. The quasi-static validation consists of experiments on a pulsator test bench which applies a normal load on the tooth flank to determine the separation diameter between the effective tooth deformation, respectively stiffness, and the gear body. By applying strain gauges on both planar sides of the gear body, the distribution of the deformation along the radius of the gear body under a quasi-static load is obtained. The wheel body shapes and the macro-geometry of the gears for the dynamic tests differ from those for the pulsator tests. Step 3 and step 4 pursue different validation objectives, see Fig. 4. While the pulsator tests are used to determine the separation diameter between tooth stiffness and gear body stiffness, the dynamic tests pursue the model validation of the dynamic excitation behavior. The respective calculation paths are independent of the gear body shape or the gear macro-geometry and can therefore be validated separately. This will allow to validate the considered eMBS modeling methods with respect to their accuracy on modeling the static gear body stiffness. Secondly, within the dynamic analysis, speed runups of a single helical gear stage are conducted to evaluate the dynamic excitation behavior as well as to obtain the dynamic system response as a foundation for a subsequent validation. The system's dynamic behavior is evaluated in terms of relative angular accelerations, structure-borne sound at the bearing seats and at sound radiating surfaces as well as airborne sound. Within the last part of the solution, simulated and measured resonance frequencies of the system as well as order levels are compared, the influence of gear body flexibility and load on these factors is evaluated and suitable modeling approaches for calculating resonance frequencies, order levels of the first gear mesh orders and for higher orders are derived. On the one hand, this provides the design engineer with a guide on suitable model fidelity levels of gear mesh excitations in NVH models based on experimental, comparable validation. On the other hand, this allows model developers to benchmark their gear mesh models against the same setup and data to comparably show disadvantages and advantages of different modelling approaches.

5 Application to a helical gear stage

Within this chapter, the solution approach described in Sect. 4 is applied to a helical gear stage. The section is structured along the steps of specification of the case-study, experimental analysis, modeling and model validation.

5.1 Specification of case-study

In order to achieve the research objective of validating the methods for simulating gear excitation in an elastic multibody simulation environment, various test gears and detailed investigation methods are used in this case study. The test gears for the quasi-static pulsator tests and the dynamic tests are presented as follows.

For the static pulsator tests, gears were selected and modified for the tests. Strain gauge chains, which consist of several equidistant measuring units, were used to prepare the gears in order to record the strain curve along a tooth. The

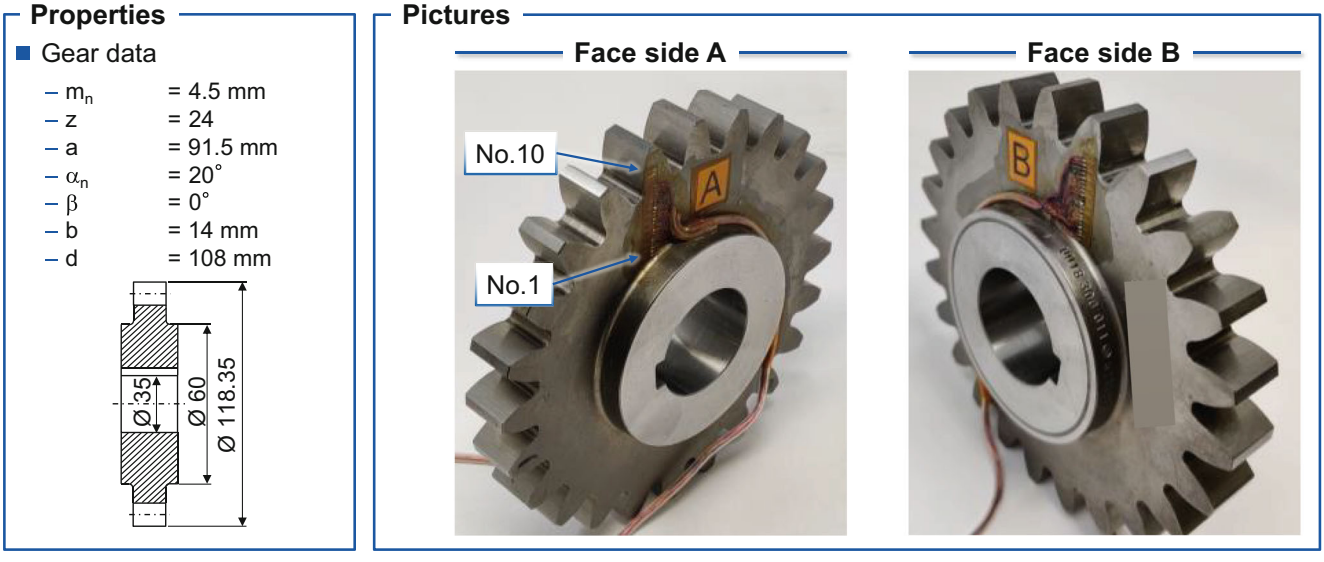


Fig. 5 Application of the strain gauges on the test gear

used gear is shown in Fig. 5. The aim is to determine the energy diameter between the tooth ring and the wheel body. A finite element simulation (FE simulation) was carried out in advance to evaluate the deformation state along the tooth into the wheel body in order to determine a suitable positioning of the strain gauge, which is defined by large strains in the tooth to allow best signal to noise ratios. To correctly record the strain conditions, the strain gauge chains were not attached to the neutral fiber of the bending tooth but positioned further outwards to the flank profile subjected to tensile stress. Figure 5 shows a prepared gear in which the tooth to be loaded is fitted with a strain gauge chain on both sides.

The measuring points were extended by a supplementary resistor to form a half-bridge within a connection box and completed with a full-bridge circuit consisting of three NI 5237 measuring cards from NATIONAL INSTRUMENTS coupled together. To assign the measurement data, the individual measurement points were named from strain gauge No. 1 to strain gauge No. 10, with strain gauge No. 1 being closest to the center of the gear and strain gauge No. 10 being furthest away.

The dynamic tests focus on investigating the excitation behavior and resonance frequencies of different gear body variants under realistic operating conditions. These investigations are crucial for validating the method for simulating gear excitation in an elastic multi-body simulation environment (eMBS). Three variants of gear sets are used, which differ in the shape of the gear body:

1. solid steel body
2. I-shaped gear body
3. C-shaped gear body

The variants allow a differentiated analysis of the influence of different gear body geometries on the dynamic excitation behavior. The dimensioning of the gear bodies was based on the design method for lightweight gear bodies according to NIEMANN-WINTER [42]. For the initial calculations, the dimensions for bar width b_s, ring thickness h_j and hub diameter d_N were initially selected conservatively. The wheel body dimensions were successively reduced so that the influence of the wheel body geometries in test bench operation on the contact stiffness and load distribution across the width is as great as possible. For the final design, the geometry dimensions were approximated in accordance with the "lightweight design" according to NIEMANN-WINTER. The bar width $b_s = 10$ mm, ring thickness $h_j = 8$ mm and the hub diameter $d_N = 65$ mm correspond to the final wheel body dimensions. A final strength verification for the wheel bodies in accordance with FKM ensures that the dynamic forces acting on the rib and the connection between the rib and shaft is permanently within the fatigue limit [43]. The wheel body geometries investigated are shown in Fig. 6. They use a common macro- and micro geometry so that the excitations induced by varying stiffness of the tooth ring are comparable.

The gear variants with different wheel body geometries were analyzed and selected in the design with regard to their operational behavior by calculating the gear mesh stiffness, the linear load distribution, the load-free rotational transmission error and the fluctuation range of the total rotational transmission error. The simulations of the parameters under consideration were carried out using the tooth contact analysis method FE-Stirnradkette STIRAK [25].

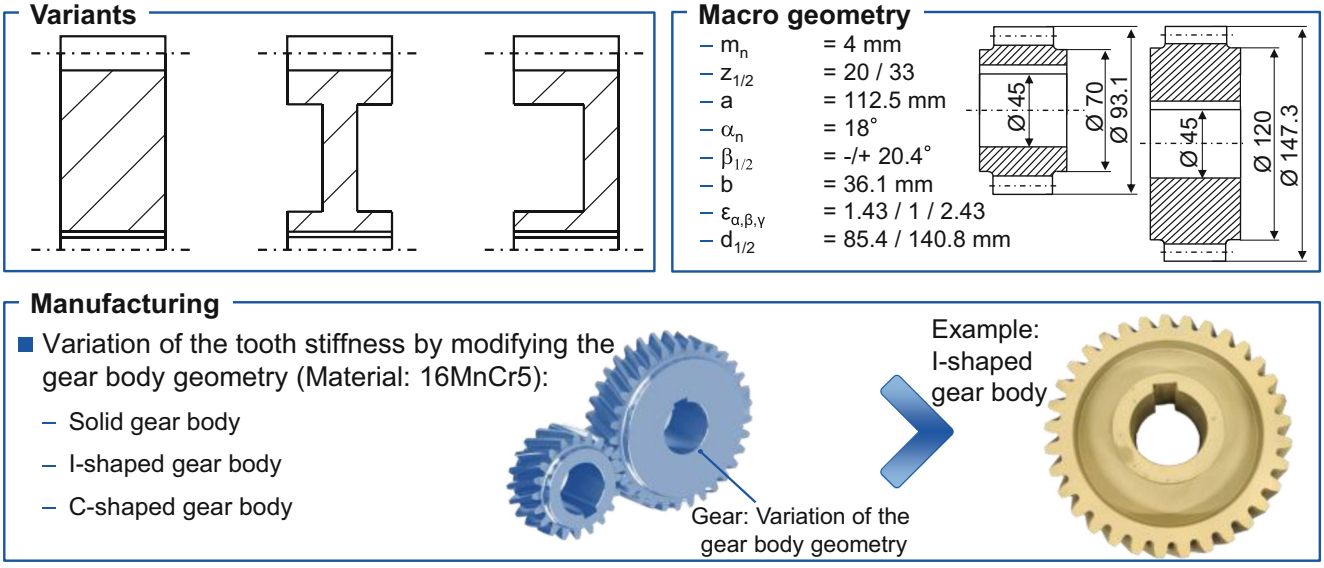


Fig. 6 Used gears for the dynamic tests

5.2 Experimental analysis

The experimental investigations are divided into two test cases according to the validation strategy. On the one hand, quasi-static pulsator tests are carried out in which the test gears are statically loaded in order to determine the strain on individual teeth. On the other hand, dynamic speed run-ups of a single-stage test gearbox are carried out to determine the structural-dynamic behavior of the overall system.

5.2.1 Quasi-static pulsator tests

For the quasi-static tests on the pulsator test rig, the focus is on measuring the strain curve along a tooth in the wheel body. The data will be used to validate the calculation of the energy diameter between the teeth area and the gear body, which will be utilized in more detailed calculations in eMBS. The separating diameter is used in the eMBS to divide the area between the flexible teeth part and the rigid gear body part. The utilized test setup is shown in Fig. 7.

The test sequence begins by adjusting the contact pattern to set a balanced line of action of the tooth clamped at the top and bottom in the pulsator, see pressure distribution in Fig. 8. The teeth are aligned centrally between the pulsator jaws. In the next step, the strain curve is measured under quasi-static load.

For the tests an electromagnetic resonance pulsator was used. It was clamped between four teeth in order to introduce the forces along the line of action and thus set realistic meshing conditions. Different tests were conducted with static forces between $F_{stat} = 2$ and 25 kN. After reaching each specified force level, a five-second measurement was carried out at a sampling rate of $f_{meas} = 50$ kHz. After reaching the maximum force of $F_{stat} = 25$ kN, the gear was released from the clamping device and clamped again in order to carry out repetitive measurements. A total of three measurements were carried out per force level for each side of the gear (A and B). The evaluated strain measurements show an increase in strain depending on the positioning between the measuring point and the pulsator force applied, ref. Fig. 8. At side B, a change in the gradient can be seen at strain gauge No. 8; the gradient of the strain decreases in comparison to the previous measuring points and in comparison to side A.

Differences in the measured strains between sides A and B could be explained by slight differences in position during the application of the strain gauge chains. Manual processing steps such as adhesive bonding and different boundary conditions due to the quantity of adhesive and curing processes also had a slight influence on the results. For this purpose, tests were carried out in which the gear teeth were clamped between the pulsator jaws in the reversed direction. The strains show plausible curves below the tooth root. Quantitatively, the strains between strain gauge No. 1 and strain gauge No. 8 for side A and side B are at a comparable level. Overall, the measurement results are in good repeatability.

In conclusion, it can be stated that the strain behavior can be measured reliably and with good accuracy in the experiment. The measured data are essential for further use in the eMBS and provide a basis to the validation of the calculation method in Sect. 5.3.

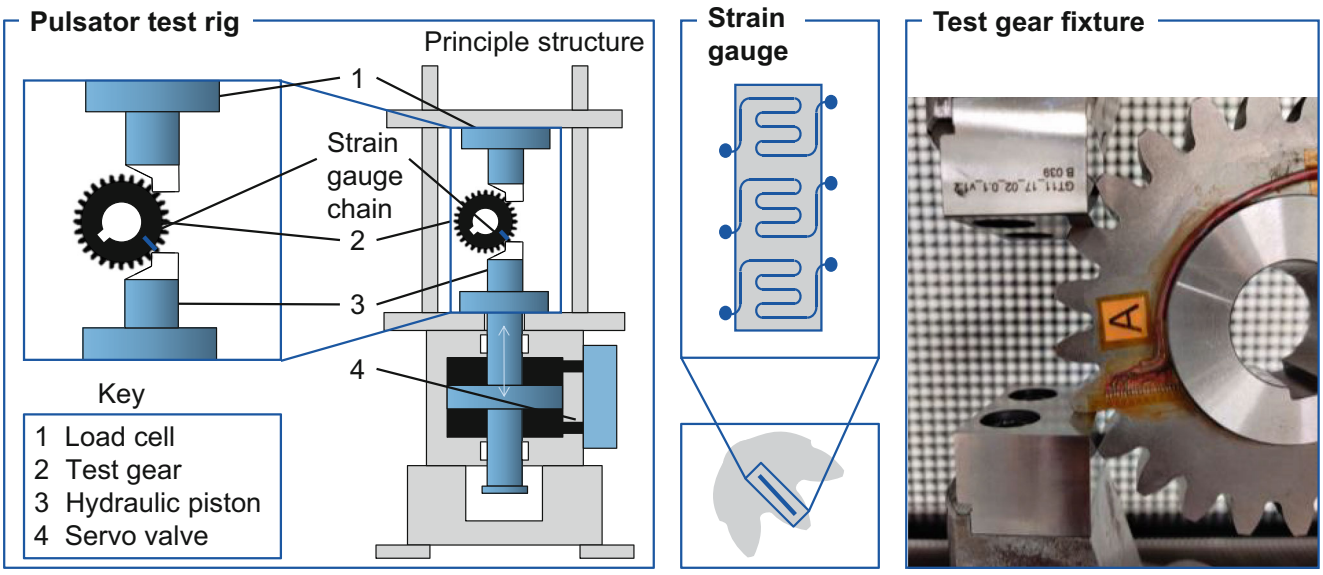


Fig. 7 Experimental principle of the quasi-static pulsator tests

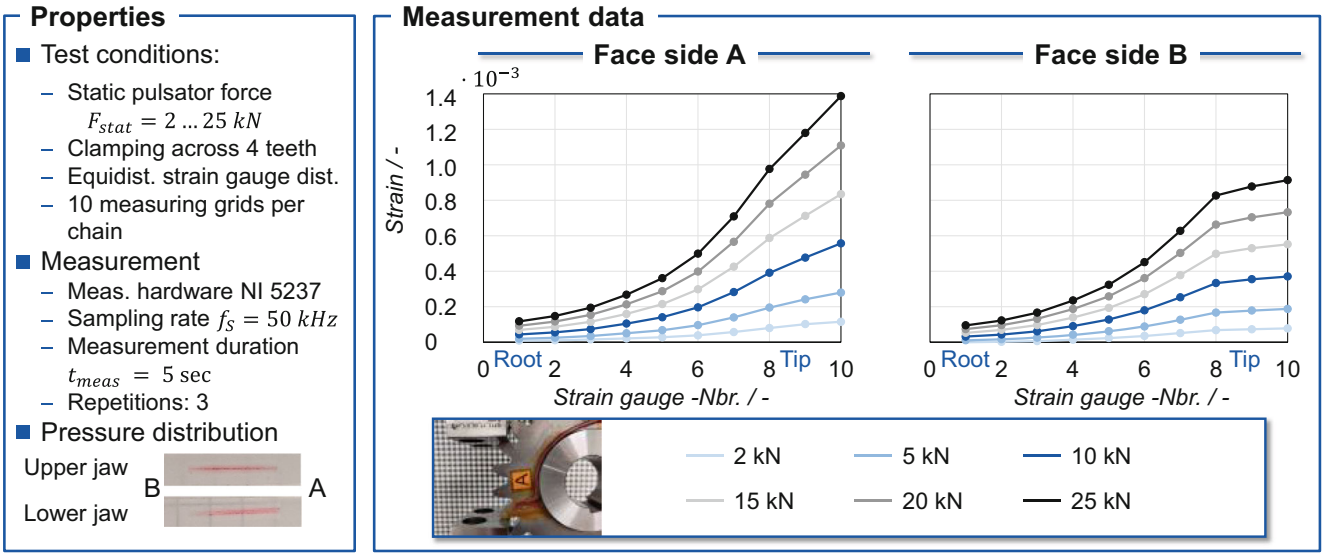


Fig. 8 Strain measurements on the pulsator test rig

5.2.2 Dynamic tests

The dynamic tests are carried out on a gearbox test rig. The test rig consists of an electric drive motor with a power output of $P_1 = 220\,kW$, a maximum speed of $n_1 = 6600\,rpm$ and a maximum torque of $M_1 = 380\,Nm$ and two electric output motors, each with a power of $P_2 = 155\,kW$, a maximum speed of $n_2 = 2500\,rpm$ and a maximum torque of $M_2 = 1300\,Nm$. The drive train for holding the measuring cell is set up in an anechoic chamber on a vibration-decoupled clamping field, while the electrical machines are located outside this chamber. The topology of the test rig is shown in Fig. 9. The test gearbox with the gears to be tested has a modular design so that the test gears can be changed quickly and without axle misalignment. A circulating lubrication system with external heating ensures a constant supply of oil at a steady temperature. An axle drive splits the drive power evenly between the two output machines. A torsional flexible coupling decouples the test cell from the axle drive in terms of torsional vibration.

The measured signals are chosen along the sound propagation chain, which describes how the sound propagates through the system from the location of the excitation at the gear mesh via the bearings to the sound-radiating surfaces. Seven triaxial acceleration sensors record structural vibrations at various positions on the gearbox housing: in

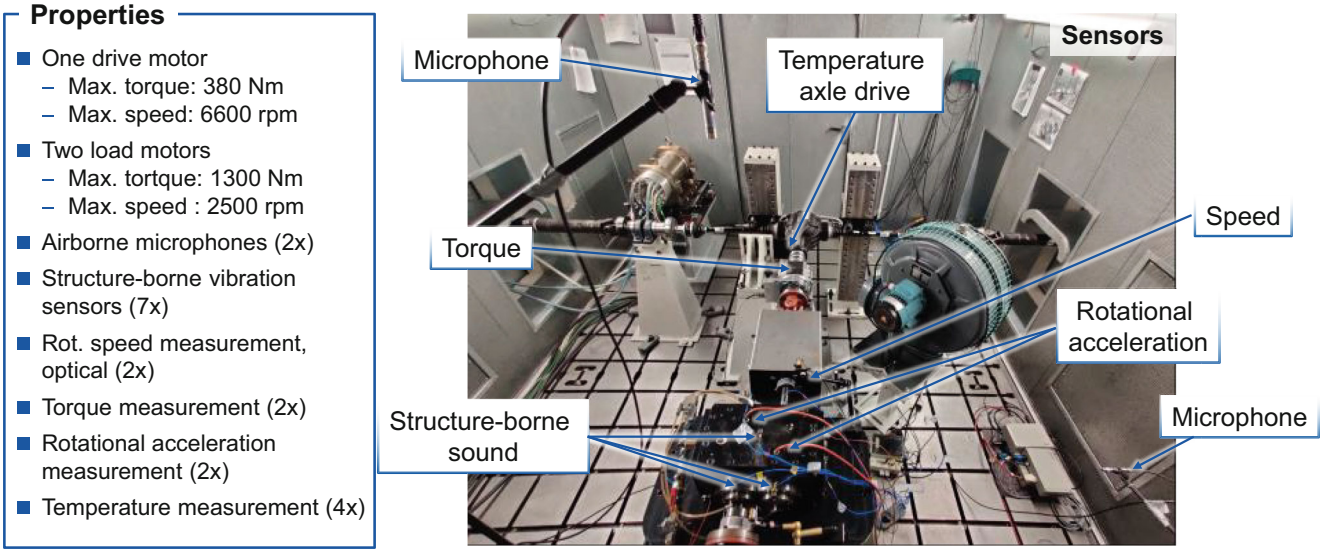


Fig. 9 Test rig setup for the dynamic tests

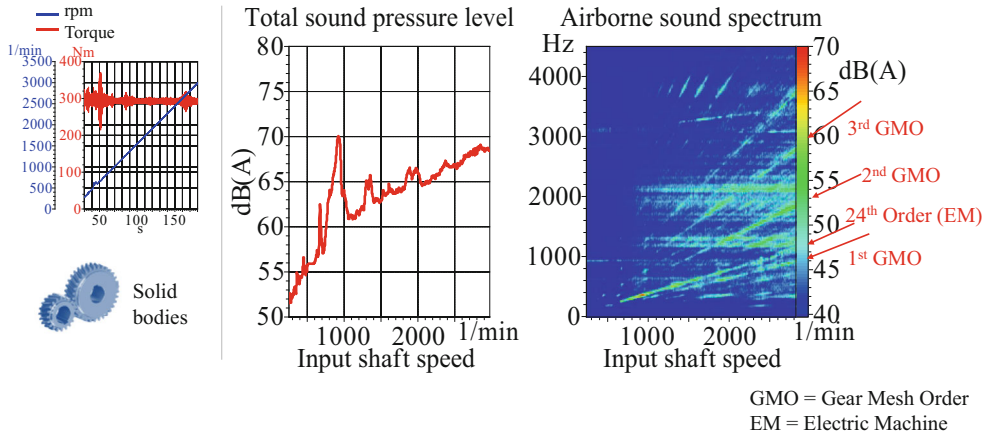


Fig. 10 300 Nm runup of solid gear bodies

the center of the housing cover, on the short side plates of the housing and on the end faces of each bearing bush near the shaft bearing. Optical speed measurements by laser are carried out on both the drive and output sides. Two microphones record airborne noise above and to the side of the gearbox at a distance of one meter from the housing surface.

The test plan consists of four blocks, which are applied to each gear variant (solid body, I-body and C-body):

- Warm-up procedure
- Speed run-ups, drive flank loaded, several constant torque levels
- Speed run-ups, coast flank loaded, several constant torque levels
- Speed and torque run ups

At the beginning of each test run, a warm-up procedure is carried out to ensure nearly identical starting conditions. The external oil unit heats the oil to a constant supply temperature of $T_{oil} = 75\,°C$ with a simultaneous operating point of $n_1 = 1100\,rpm$ at $M_1 = 250\,Nm$ until a housing temperature between $T_{housing} = 55\,°C$ and $T_{housing} = 58\,°C$ is reached. The measurement procedure consists of speed and torque ramps: First, speed run ups with a constant gradient between $n_1 = 300$ ... 3000 rpm. The evaluated torque levels later in this section are at full load ($M_1 = 300\,Nm$) and partial load ($M_1 = 25\,Nm$) for the drive flank. These testing steps were each repeated three times to ensure the reproducibility of the measurement results. During this time, the operating temperature was continuously monitored; cooling phases were inserted if necessary. The structural dynamic results obtained from the experimental setup are presented in what follows. Figure 10 shows the airborne sound recorded $s = 1\,m$ above the gear box housing during a speed runup with a torque of $M_1 = 300\,Nm$ at the input shaft. The total level shows resonance peaks at $n_1 = 900\,rpm$, 1250 rpm, 2000 rpm and above 2500 rpm with a maximum of 70 dB(A) as well as an increase of the sound pressure level from 52 dB(A) at $n_1 = 300\,rpm$ to 65 dB(A) at $n_1 = 2500\,rpm$. The frequency spectrum shows that the resonances below 1500 rpm are excited by a 24th order which can be attributed to the number of pole pairs of one of the driving machines of the test bench. However, the resonances at $n_1 = 2000\,rpm$ and above $n_1 = 2500\,rpm$ are related to the second gear mesh order and occur at natural frequencies of the system at $f_0 = 1360$ and 1900 Hz, respectively. These two points are therefore chosen as the ones to be studied in the following, because the exceedingly high sound pressure levels below 1500 rpm are not excited by the gear box under test, but by test bench control and are therefore not suitable for analyzing the model quality. This can be identified by looking at the excitation orders: the 24th order, which excites the resonances at e.g. 900 rpm, does not match the 20 teeth of the pinion and is therefore not related to the gear box, but can be attributed to the driving machines.

The comparison of the structure-borne sound (ref. Fig. 11) with airborne sound reveals that the acceleration observed at the sensor at the bearing seat of the drive shaft on the driving side in axial direction resembles the airborne sound the most: Both resonances of the second gear mesh order can be identified at $n_1 = 2000\,rpm$ and above $n_1 = 2500\,rpm$ in the acceleration signal. This allows to focus the analysis of influencing factors on the acceleration measured, enabling a model validation in structure-borne sound.

The influence of torque and gear body variant on the dynamic system behavior is shown in Fig. 12. Especially with a variation of the gear body, shifts in the resonances can be observed. These shifts in resonances have two possible causes: On the one hand, eigen frequencies may vary because of different masses, loads and load-dependent stiffness. On the other hand, the load distribution changes in the gear mesh contact, causing a change in excitation orders. With more prominent higher orders, resonances occur at different eigen frequencies. Both effects are studied in what follows.

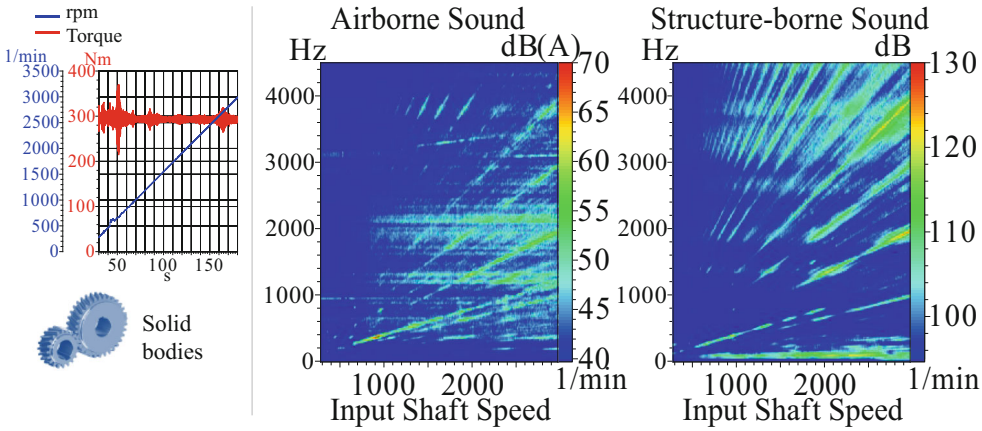


Fig. 11 Comparison of airborne sound and structure-borne sound at full-load speed runup of solid gear bodies

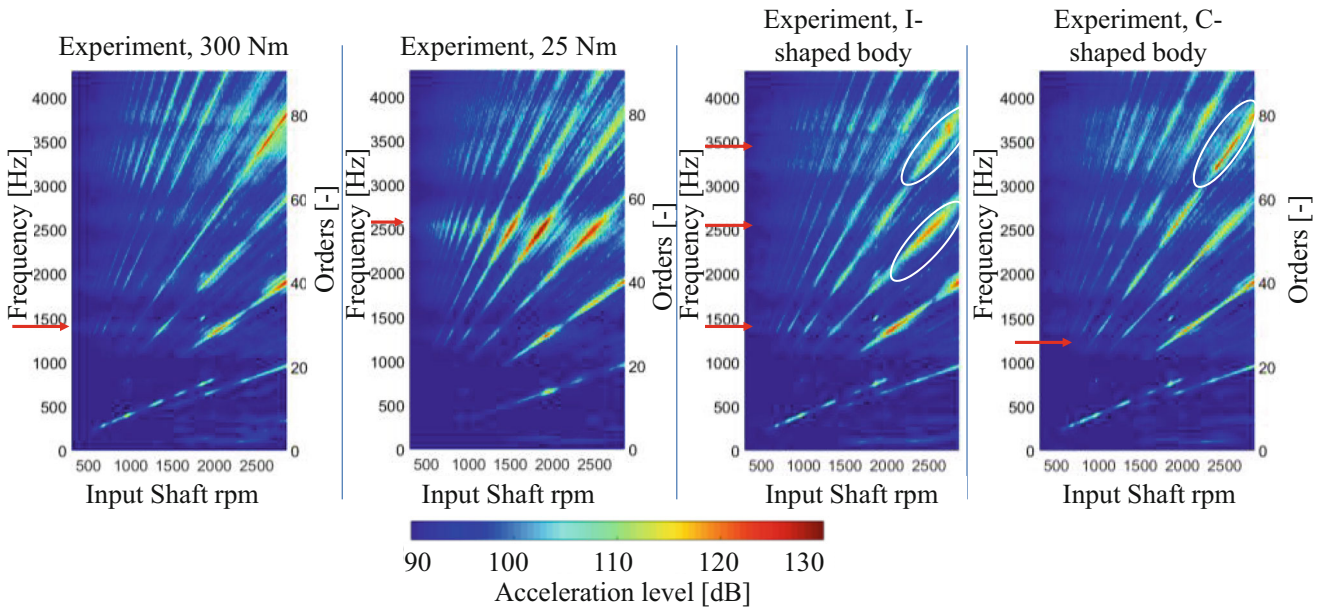


Fig. 12 Comparison of structure-borne sound at bearing seat of drive shaft in axial direction under **a** full-load speed runup, **b** $M_1 = 25\,Nm$ torque speed runup, **c** full-load speed runup with I-shaped gear body, **d** full-load speed runup with C-shaped gear bodies

When comparing the full-load speed runup at $M_1 = 300\,Nm$ torque with the lowest torque runup at $M_1 = 25\,Nm$ torque, the dominant resonance shifts: While the natural frequency at $f_0 = 1360\,Hz$ is still excited by the second gear mesh order, the highest amplitudes occur when one of the higher-order excitations coincides with a natural frequency at $f = 2600\,Hz$. Also, the absolute peak amplitudes during resonance are about $\Delta L_h = +5\,dB$ larger than at full load ($L_h = 131\,dB$ compared to $L_h = 126\,dB$). Furthermore, the 4th, 5th and 6th gear mesh excitation order are more prominent during low-torque operation, than at full-load.

In comparison, the natural frequencies shift little with a change in gear body geometry. All three resonances observed at either $M_1 = 300\,Nm$ or $M_1 = 25\,Nm$ input torque and solid gear body are also visible both in the I-shaped as well as the C-shaped gear body. However, a change can be observed in the excitation behavior of the gear stage, which is caused by different contact properties, possibly different load distributions induced by the gear wheel flexibility. Specifically, the third excitation order of the measurements with the I-shaped gear body is exhibiting a resonance of $L_h = 122\,dB$ at $f_0 = 2600\,Hz$, which is not visible with the solid body. On the other hand, the dominant resonance with the C-shaped gear body occurs above $f > 3\,kHz$ and is excited by the 4th gear mesh order, while the resonances excited by the second gear mesh order are comparable with the resonances of the solid gears with $L_h = 125\,dB$ in peak amplitude. All three gear variants show comparable side bands around the resonances of the second gear mesh order. These side bands can be correlated to the rotation of the slow shaft and may indicate eccentricities of the shaft axis.

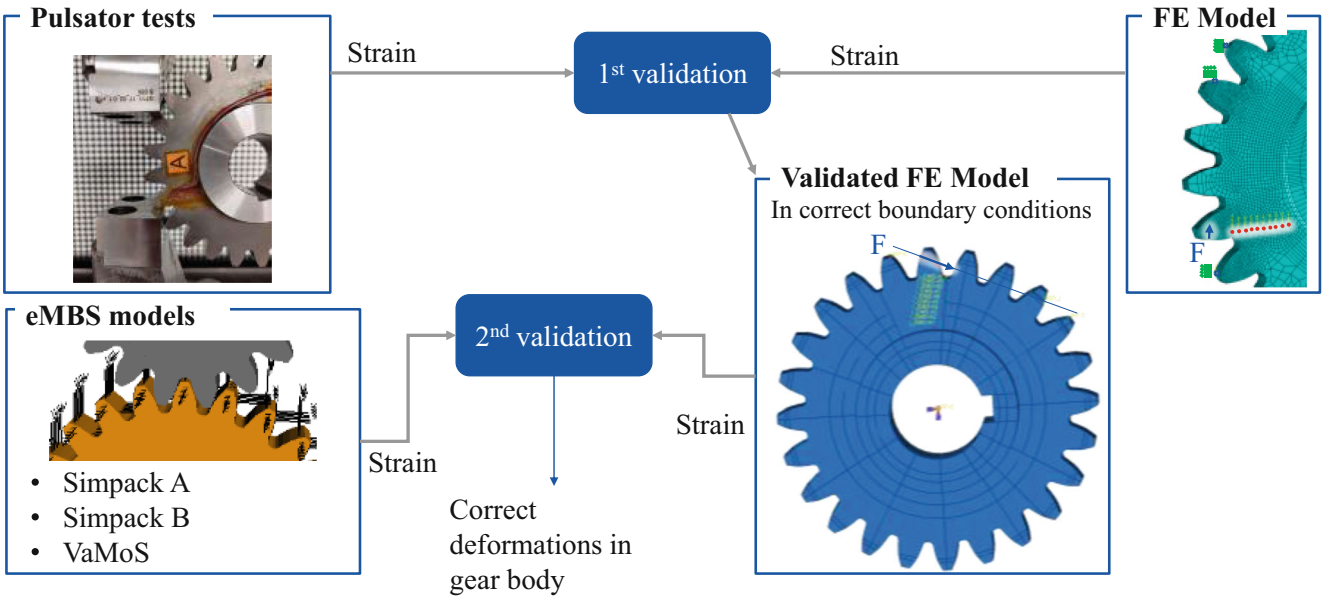


Fig. 13 Process for quasi-static validation

In conclusion, the dynamic experimental analysis shows a shift in critical natural frequency of $f_0 = 1360\,\text{Hz}$ at full load and with solid gears during a change in torque as well as gear body geometry. The influence of the load exceeds the influence of the gear body by 4 dB. The structure-borne sound observed serves as a basis for the subsequent model validation.

5.3 Modeling & model validation

The aim of the model generation is to supply a basis for validating both the quasi-static and the dynamic behavior of the gear model. Firstly, the quasi-static modeling and validation is described. The validation is based on the strains obtained from the pulsator tests, described in Sect. 5.2. The process for quasi-static validation is shown in Fig. 13. The experimentally obtained strains along the diameter of the gear body are used to validate an FE-Model of the gear, replicating the boundary conditions and force application of the test bench. The validated FE-Model is then used as a reference model for validating the eMBS modeling variants. This two-step approach is necessary, because the boundary conditions in the test setup differ from the ones in a meshing gear: The pulsator induces a force along the line of action at two different teeth. The second pulsator jaw supports the reaction force on the second tooth. However, in a meshing gear more than one tooth is on contact with the meshing gear and the resulting torque is supported via the connection between gear and shaft. As the eMBS modeling approach is only capable of representing one gear mesh contact, it can only be compared to an FE model of one individual contact, which requires the corresponding gear to be fixed to the shaft.

Figure 14 shows the results of the quasi-static validation. In Fig. 14a, the comparison between measured strains on the two planar sides of the gear body and the strains simulated from the FE model is shown. The strains are depicted in dependence of the strain gauges No., ranging from 1 for the strain gauge at the smallest diameter well below the foot diameter until no. 10 which is situated at the largest diameter close to the pitch diameter. The change from gear body to tooth occurs between DMS no. 8 and 9. It can clearly be seen that the simulated and measured strains are in good agreement within the gear body with deviations of less than $p < 6\%$. However, in the tooth, the difference between simulation and measurement increases to $p = 50\%$. The comparison of the nominally identical two sides of the gear body shows that this deviation is caused by the sensitivity of the strain gauges towards the position tolerance during application. Therefore, the model's error is within the measurement reproducibility. As the main goal of the quasi-static validation is to validate the deformation within the gear body, as this is the important deformation for the sound propagation through the shaft and the bearings to the sound radiating surfaces of the housing, the FE-model will be considered valid for evaluating the modeling error introduced by different eMBS modeling methods.

Figure 14b shows the comparison of strains of the FE model with strains from the studied eMBS model variants. The comparison is done separately for the gear body and the tooth. Within the gear body (DMS no. 1–8), the methods in SIMPACK (SIMPACK 225 A and B, tooth calculation according to WEBER/BANASCHEK) and the VAMOS-method

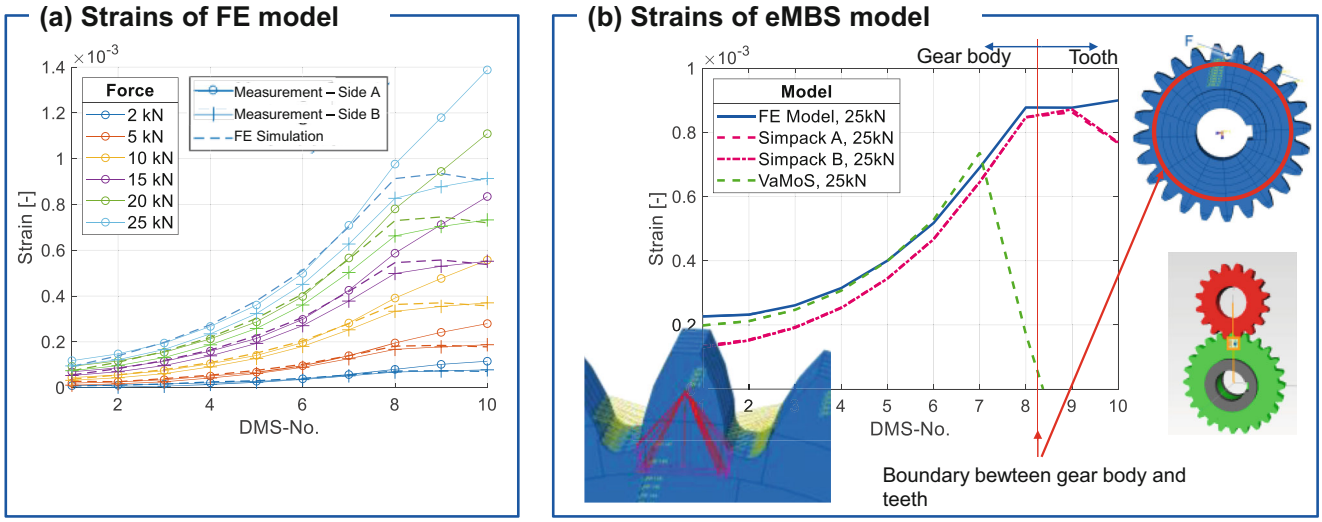


Fig. 14 Quasi-static validation

yield qualitatively compatible strains to the FE-model with a progressive increase of strain with an increase of diameter. However, the quantitative error with the VAMOS method is only $p = 12\%$, while both SIMPACK models yield errors of up to $p = 43\%$. On the other hand, the VAMOS method, which is designed to neglect the deformation of the tooth in the modally reduced body and instead consider it from the pre-calculated stiffness arrays, shows no significant strain in the tooth, while both SIMPACK methods capture the tooth strains within $p = 3.5\%$. As the main goal of the simulation method is to accurately capture the strains within the gear body to model the effect of gear stiffness variations on the deformation of gear and shaft, the VAMOS method is validated and considered more precise than the SIMPACK method. However, if accurate representation of tooth strain and stress is required in eMBS, the SIMPACK methods are better suited. The comparable SIMPACK results are remarkable, as the difference between the two methods is a different coupling of the flexible nodes in the FE model to the flexible body (SIMPACK A at tooth root, SIMPACK B at the operating pitch diameter) which results in different approaches for considering tooth bending in the tooth mesh calculation. While SIMPACK A considers tooth bending by the Weber-Banaschek approach, SIMPACK B calculates the tooth bending stiffness using the flexibility of the modally reduced Gear bodies. However, a difference in gear mesh stiffness at a constant load should not significantly influence the deformation of the gear body under constant load. Therefore, although the tooth mesh calculation approach is different, similar strains in the gear body appear plausible.

Based on the validated quasi-static models, the dynamic modeling is executed. Its aim is to model both the gear-mesh excitation as well as the system's response and the interaction between shaft oscillations and gear mesh excitations. Therefore, the eMBS model is created in time-domain, which is required to model the non-linear interaction between shaft oscillations and gear mesh excitations as seen in the measurement (ref. Section 5.2) as side bands. Figure 15a shows the eMBS model. It consists of modally reduced parts of the housing, the driving shaft and the driven shaft. The model is built in the eMBS software SIMPACK. The shafts are supported in the housing using force elements which calculate the non-linear bearing stiffness based on the HERTZIAN contact theory. The speed runup is applied on the driving shaft and the torque is applied on the driven shaft. All three models are using the same design values for macro- and micro geometry for calculating the gear mesh stiffness.

Figure 15b shows the validation of the housing model in the frequency domain with an experimental modal analysis and shows average errors of $e = 3.0\%$ in the frequency range until $f_0 = 3\,\text{kHz}$ and of $e = 3.24\%$ in the frequency range below $f < 5\,\text{kHz}$. Therefore, the model can be considered valid with respect to the natural frequencies of the housing and is therefore suitable to evaluate the effects of gear mesh excitations in the structure-borne sound at both the bearing seats as well as the radiating surfaces.

Figure 16 shows the comparison of structure-borne sound at the bearing seat of the input shaft in axial direction at the maximum input torque of $M_I = 300\,\text{Nm}$ during runup for solid gear bodies. This case is selected as the reference case as it transmits the highest torque and the acceleration location corresponds the most to the measured airborne sound.

All simulation models exhibit similar natural frequencies both compared to each other and compared to the measurement with a maximum deviation of $p = 11\%$ between simulation and measurement at the first natural frequency.

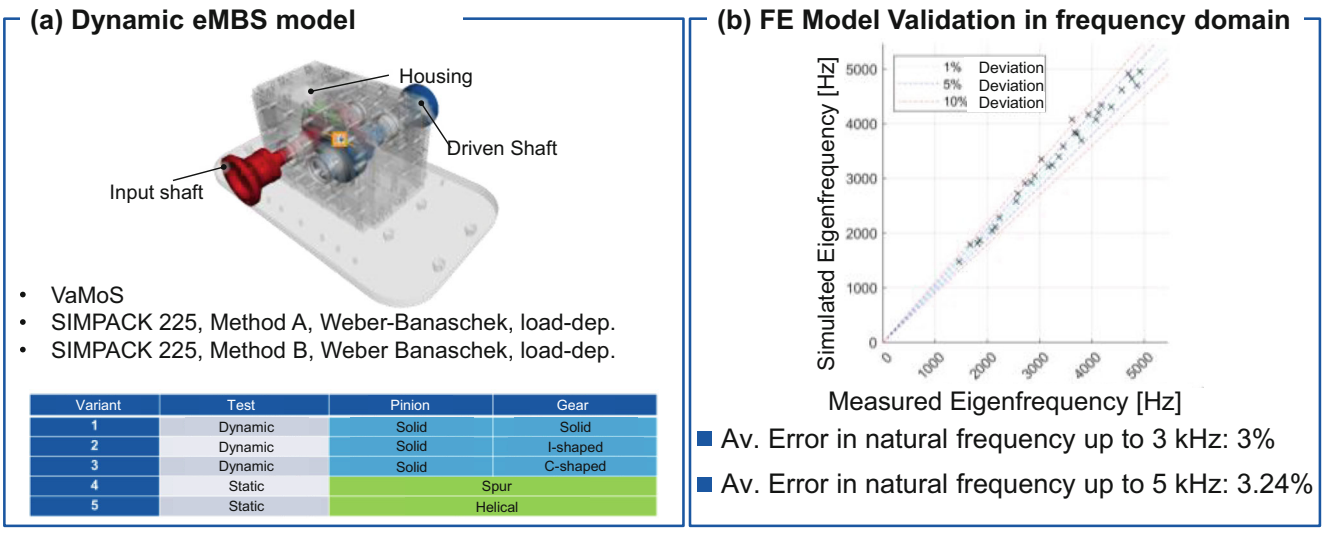


Fig. 15 **a** Dynamic model and **b** validation in frequency domain

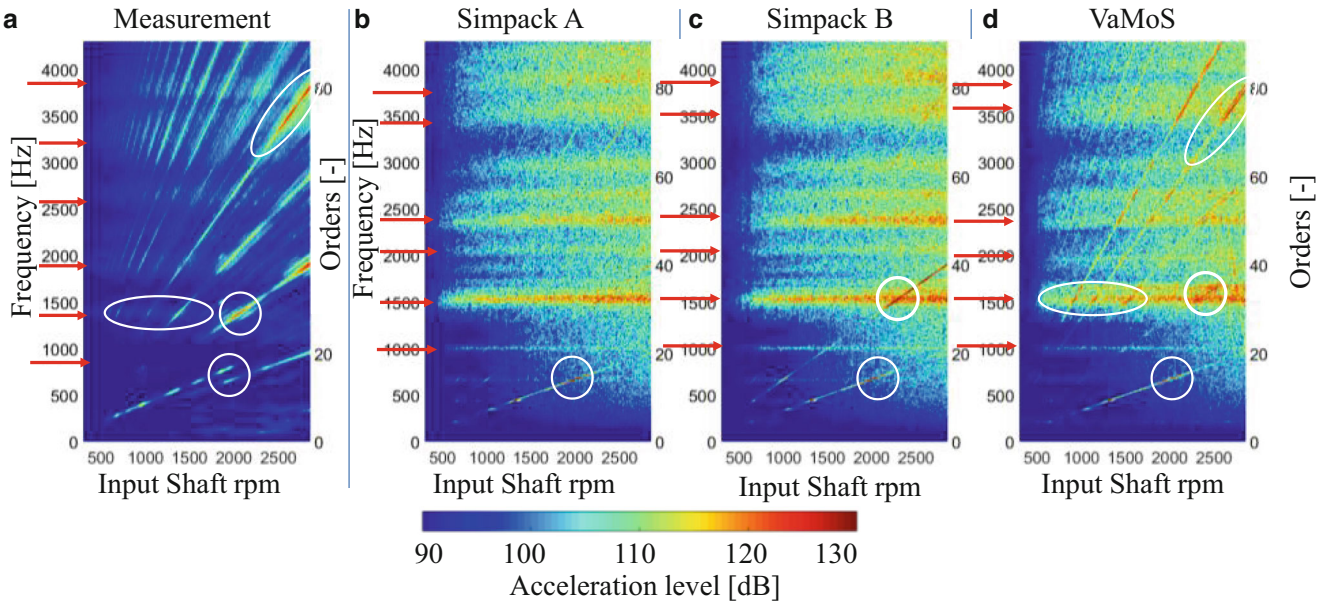


Fig. 16 Structure-borne sound at bearing seat of input shaft in axial direction. **a** Measurement, **b** Simpack A, **c** Simpack B, **d** VaMoS. Gear stage with solid gear bodies. $M_1 = 300\,\text{Nm}$ torque

However, all simulation models exhibit higher acceleration levels than the measurement, as the damping in bearings and in the gear mesh could only be assumed during modeling. When comparing the excitation orders, the modeling approach according to SIMPACK A is capable of replicating the first gear mesh order observed during experiment (20th shaft order), but no higher-order excitations are captured. Therefore, there is only one resonance observed both in measurement and simulation, at $n_1 = 2000\,\text{rpm}$ and $f_0 = 670\,\text{Hz}$, dominated by the first gear mesh excitation. All resonances at higher frequencies are not dominated by gear mesh excitations, but by numerical background noise exciting all natural frequencies. In contrast, SIMPACK B indicates the most critical resonance at $n_1 = 2200\,\text{rpm}$, when the second gear mesh order coincides with the $f_0 = 1550\,\text{Hz}$ natural frequency and therefore significantly improves the accuracy of the simulation results. However, no higher orders than the second gear mesh order are calculated using the SIMPACK B approach. Only with the VAMOS method, all higher-order excitations observed in the measurement are calculated. Therefore, the resonances at $f_0 = 1550\,\text{Hz}$ in the speed range between $n_1 = 500\,\text{rpm}$ and $n_1 = 1500\,\text{rpm}$ are only modeled correctly using VAMOS, which consists of pre-calculated stiffnesses arrays. Additionally, the resonance of the

4th gear mesh order at $f_0 = 3500$ Hz and $n_1 = 2750$ rpm is also only calculated by the VAMOS method. This is an indication that the use of a numerically pre-calculated gear mesh stiffness is more suitable for modeling higher-order excitations in time-domain NVH simulations, than the approaches according to WEBER-BANASCHEK, which are used in both SIMPACK A and SIMPACK B.

Subsequently, the influence of load and gear body geometry is studied. Firstly, Fig. 17 shows the influence of load, comparing the measurement results with the VAMOS calculation results. Both in measurement and simulation, the resonance with the highest amplitudes shifts from around $f_0 = 1500$ to 2500 Hz. The resonances are excited in measurement and simulation by the third, fourth, and fifth gear mesh order. Also, the reduction in resonance amplitude of the fourth gear mesh order is visible in simulation and measurement. Overall, the effects of different loads observed in the measurement are well captured in the VAMOS method. Furthermore, the increased acceleration level of $L_h = +5$ dB at $M_1 = 25$ Nm input torque compared to 300 Nm input torque is also captured using the VAMOS method.

The comparison of the studied eMBS simulation models with respect to their accuracy in capturing the effect of load variations is shown in Fig. 18. While all simulation models show resonances excited by higher orders, only the VAMOS method is capable of identifying all critical resonances at 2500 Hz (highlighted in the white circle in Fig. 18). Both SIMPACK A and SIMPACK B exhibit multiple gear mesh orders exciting resonances simultaneously at $n_1 = 2500$ rpm, but no resonances at $n_1 = 1500$ rpm and $n_1 = 1000$ rpm at 2500 Hz. Additionally, the second gear mesh order is significantly over-estimated by both SIMPACK methods compared to the measurement, while the resonance at 1350 Hz and $n_1 = 2000$ rpm is not predicted by the VAMOS model. Overall, the most significant higher order resonances are again, equivalent to the analysis at full load, only modeled accurately with the VAMOS method.

The influence of altering the gear body variant is exemplarily discussed by comparing the solid gear body with the I-shaped gear body at full-torque speed runup, see Figs. 19 and 20. In Fig. 19, the change of structure-borne sound at the bearing seat of the input shaft when changing the gear body from solid to I-shaped is shown for the measurement and for the VAMOS simulation. While the natural frequencies do not change significantly in measurement and simulation, it can be seen that the resonances of the third gear mesh order at $f_0 = 2500$ Hz increase by 6 dB in the measurement. While there is also an increase of 3 dB in the VAMOS simulation, it is quantitively significantly smaller than the resonance at the fourth gear mesh order, which remains comparable between solid gear and I-shaped gear in simulation and measurement. This may be an indication that, while the modeling of the varying gear mesh stiffness using numerically pre-calculated stiffnesses seems to be better at improving high-frequency excitation behavior, it is more sensitive to the modeling of the interaction between gear body stiffness and tooth stiffness.

The comparison of the studied eMBS models in Fig. 20 shows that the critical resonance at the third gear mesh order and at 2300 Hz is calculated with both SIMPACK methods, while still not calculating the resonance at $f_0 = 3500$ Hz and

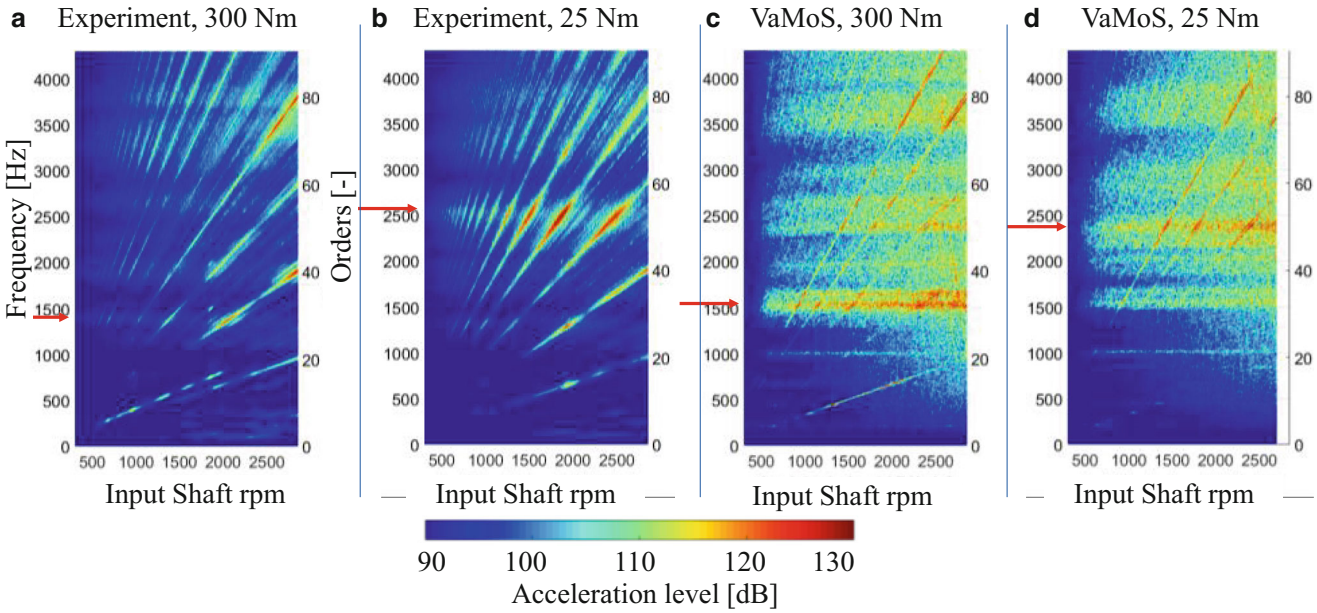


Fig. 17 Influence of torque reduction from 300 to 25 Nm on structure-borne sound at bearing seat of input shaft in axial direction. **a** Measurement, **b** VaMoS. Gear stage with solid gear bodies

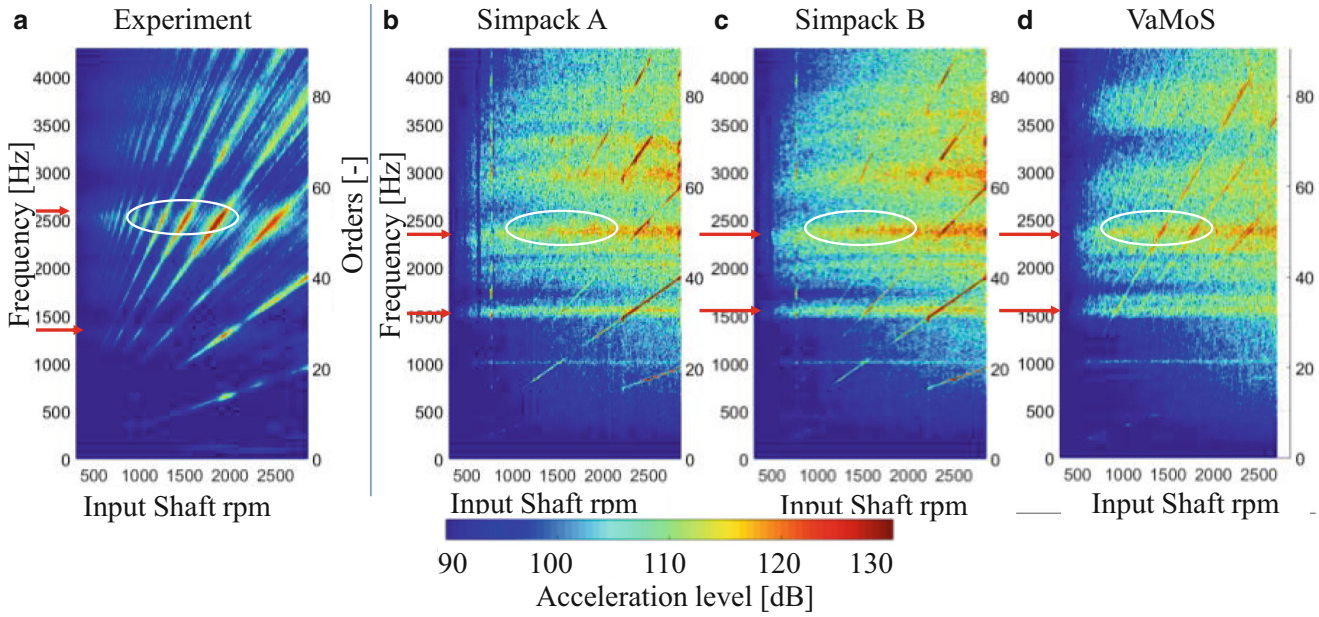


Fig. 18 Structure-borne sound at bearing seat of input shaft in axial direction. **a** Measurement, **b** Simpack A, **c** Simpack (B), **d** VaMoS. Gear stage with solid gear bodies. 25 Nm torque

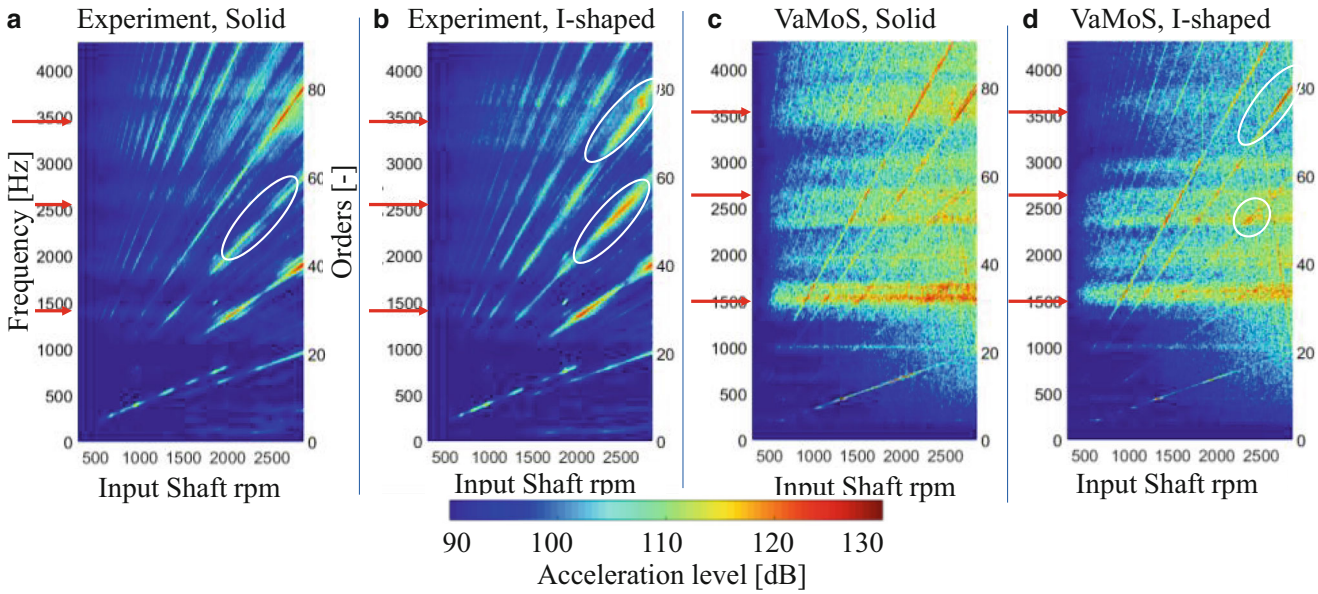


Fig. 19 Influence of I-shaped gear body compared to solid gear body on structure-borne sound at bearing seat of input shaft in axial direction. **a** Measurement, **b** VaMoS

the fourth gear mesh order, which is only calculated using the VAMOS method.

The conclusions drawn from the validation are visualized in Table 1.

With increasing accuracy of the models, the computational effort increases. While a runup using SIMPACK A is calculated within a few hours, the SIMPACK B calculation requires roughly a day and the VAMOS method a few days to generate the waterfall diagrams.

In general, it can be observed that all simulation models accurately model the natural frequencies of the studied gear box under different loads and gear body variants. However, differences occur in the excitation modeling. In the setup based on solid gear bodies and at $M_1 = 300$ Nm input torque, higher-order excitations were observed in the measurement which could only accurately be modeled with the VAMOS method, while SIMPACK A only captured the first gear mesh order and SIMPACK B only captured the

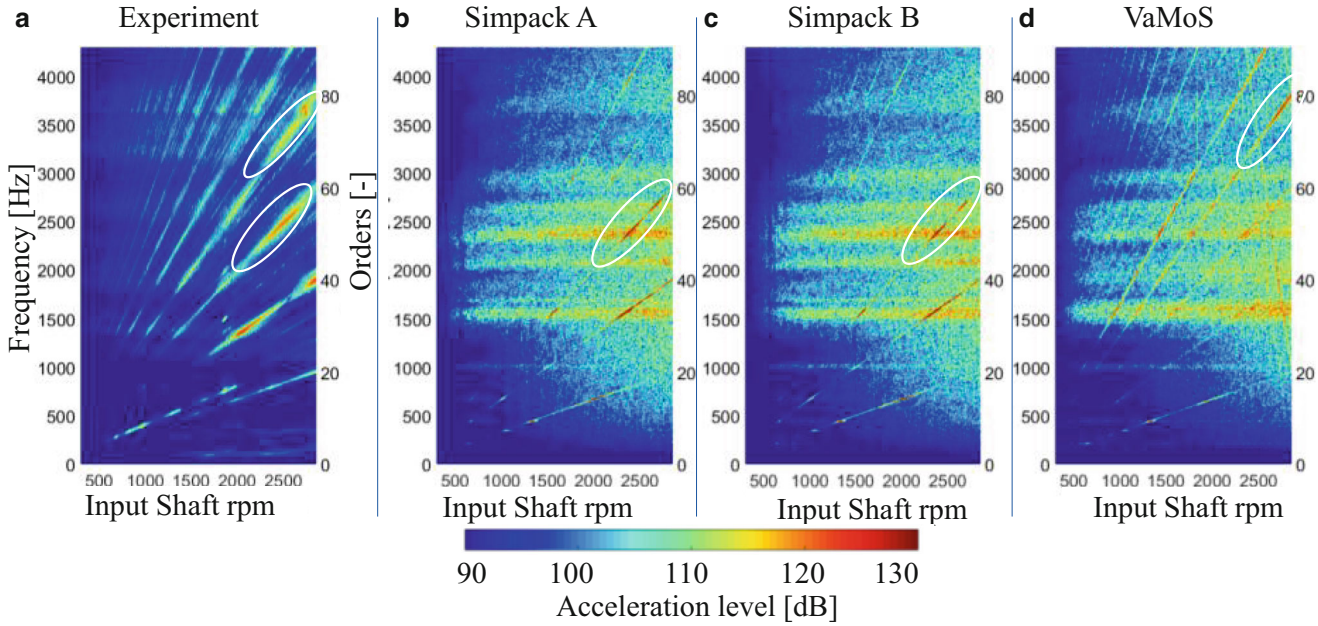


Fig. 20 Structure-borne sound at bearing seat of input shaft in axial direction. **a** Measurement, **b** Simpack A, **c** Simpack (B), **d** VaMoS. Gear stage with I-shaped gear bodies

Table 1 Validation of modeling methods for gear mesh excitations for different modeling scopes

Modeling method	Simpack A	Simpack B	VaMoS
Model purpose			
Calculation of load-dependent natural frequencies	✔	✔	✔
Calculation of natural frequencies depending on gear body variant	✔	✔	✔
Calculation of resonances of first gear mesh order	✔	✔	✔
Calculation of resonances of first and second gear mesh order	✗	✔	✔
Calculation of resonances of gear mesh orders higher than two for sold gear bodies	✗	✗	✔
Calculation of gear mesh orders higher than two for flexible gear bodies	✗	(✔)	(✔)

✔ suitable, ✗ unsuitable, *(✔)* partially suitable, i.e. some resonances are identified

first two gear mesh orders. The critical resonances at low torques of $M_1 = 25\,\text{Nm}$ were also only identified using the VAMOS model. Therefore, in comparatively rigid gears, the VAMOS method of applying a numerically pre-calculated gear mesh stiffness seems to increase the model accuracy with respect to higher-order frequency content which is crucial for simulating the acoustic behavior of gearboxes. On the other hand, the dynamic behavior of a more flexible, I-shaped gear body is partially simulated in higher accuracy using the SIMPACK methods, especially with respect to the most critical resonance at the third gear mesh order, while the higher excitation orders were again only simulated using the VAMOS method. This could indicate that in future works, combining the approach for applying forces on flexible gears used in SIMPACK and numerically pre-calculated gear mesh stiffnesses should be combined to increase the accuracy of gear mesh excitation models for NVH simulations even further.

6 Summary and outlook

Gear mesh excitations caused by a varying gear mesh stiffness are one of the most dominant excitation mechanisms in drive trains. They significantly influence the NVH behavior of drivetrains and thus have to be accurately considered in NVH system simulation models to allow for model-based optimization of gearboxes during the development process. The gear mesh stiffness is significantly influenced by the transmitted torque and interacts with the stiffness of the gear bodies, especially, if the gear bodies follow a lightweight design.

The contribution has compared and validated three high-fidelity time-domain models of gear mesh excitations with respect to the influence of load and gear body design on natural frequencies and excitation orders. The compared models are two commercially available implementations of the WEBER-BANASCHEK load-dependent stiffness calcula-

tion approach which apply the local tooth forces either at the tooth root or at the pitch diameter and are implemented in the software SIMPACK. Additionally, an approach using numerically pre-calculated stiffness arrays as developed in [6, 38] and applying the forces at a diameter defined by the strain distribution in the gear body is compared. All three methods are validated against dynamic experimental analysis of a helical gear stage.

Experimentally, during runups of the helical gear stage at constant load, a change in dominant natural frequency of 1200 Hz when reducing the load from full load of 300 to 25 Nm input torque as well as an increase of 6 dB was observed. When changing the gear body from a solid gear body to a more flexible, I-shaped gear body, the dominant resonance shifted by less than 50 Hz. Therefore, the conducted experimental dynamic analysis is suitable for observing the dynamic system behavior under different loads and gear wheel flexibilities.

All gear mesh models were able to predict the natural frequencies of the system within an error of 11%. However, while the SIMPACK approach applying forces at the tooth root was only able to model the first gear mesh excitation order, and SIMPACK B capturing the first two excitation orders, the VAMOS method is capable of modeling higher-order excitations, reducing the modeling error compared to SIMPACK models by up to 10 dB. Especially at low torques of 25 Nm, only the VAMOS method is capable of capturing the experimentally observed critical resonances caused by the third to fifth gear mesh excitation order. Therefore, on comparably rigid gears, SIMPACK A and B can be used when the first or first and second order are of interest, respectively. For higher order simulations to be accurate, the VAMOS approach should be considered.

However, with the flexible gear models, the SIMPACK B approach showed advantages in the frequency range up to 2700 Hz. Therefore, a combination of numerically pre-calculated gear mesh stiffnesses with the SIMPACK approach of applying forces on flexible bodies should be considered in the future.

Funding Open Access funding enabled and organized by Projekt DEAL.

Conflict of interest S. Wischmann, A. Mann, G. Jacobs, C. Brecher, G. Hoepfner and C. Westphal declare that they have no competing interests.

Open Access Dieser Artikel wird unter der Creative Commons Namensnennung 4.0 International Lizenz veröffentlicht, welche die Nutzung, Vervielfältigung, Bearbeitung, Verbreitung und Wiedergabe in jeglichem Medium und Format erlaubt, sofern Sie den/die ursprünglichen Autor(en) und die Quelle ordnungsgemäß nennen, einen Link zur Creative Commons Lizenz beifügen und angeben, ob Änderungen vorgenommen wurden. Die in diesem Artikel enthaltenen Bilder und sonstiges Drittmaterial unterliegen ebenfalls der genannten Creative Commons Lizenz, sofern sich aus der Abbildungslegende nichts anderes ergibt. Sofern das betreffende Material nicht unter der genannten Creative Commons Lizenz steht und die betreffende Handlung nicht nach gesetzlichen Vorschriften erlaubt ist, ist für die oben aufgeführten Weiterverwendungen des Materials die Einwilligung des jeweiligen Rechteinhabers einzuholen. Weitere Details zur Lizenz entnehmen Sie bitte der Lizenzinformation auf http://creativecommons.org/licenses/by/4.0/deed.de.

References

1. Bender B, Gericke K (eds) (2021) Pahl/Beitz Konstruktionslehre: Methoden und Anwendung erfolgreicher, 2021st edn. Produktentwicklung, vol 9. Springer Berlin Heidelberg, Berlin, Heidelberg
2. Fuchs A, Nijman E, Priebsch H-H (2016) Automotive NVH Technology. Springer, Cham
3. Drichel P, Jaeger M, Müller-Giebeler M et al (2021) Influence of Model Detail Level on the Prognosis Quality of the Perceived Sound of an Electrified Passenger Car Powertrain. Iop Conf Ser: Mater Sci Eng 1097:1–12. https://doi.org/10.1088/1757-899X/1097/1/012010
4. Pasch G, Jacobs G, Berroth JK (2020) NVH system simulation of a tractor with hydrostatic-mechanical power split transmission. Landtechnik 2020:301–315. https://doi.org/10.15150/lt.2020.3254
5. Wischmann S, Pasch G, Jacobs G et al (2023) Numerische Transferpfadanalyse zur modellbasierten Optimierung des Geräuschverhaltens von. Antriebssträngen In: Tagungsband Daga Pp: 452–455
6. Andary F, Heinzel C, Wischmann S et al (2023) Calculation of tooth pair stiffness by finite element analysis for the multibody simulation of flexible gear pairs with helical teeth and flank modifications. Multibody Syst Dyn 59:395–428. https://doi.org/10.1007/s11044-023-09926-4
7. Golafshan R, Su B, Jacobs G et al (2022) Characterization of elastohydrodynamic contact film thickness under high frequency force excitation using a 2D unwrapping-based image processing technique. Tribol Int. https://doi.org/10.1016/j.triboint.2022.107841
8. Rapp T, Jacobs G, Berroth J et al (2023) Optimization workflow to parameterize elastomer material models based on arbitrary time-domain measurement data. J Appl Polym Sci. https://doi.org/10.1002/app.53974
9. Wischmann S, Seifert K, Berroth J et al (2022) On the influence of surface sealant on the nonlinear dynamics of jointed structures. Mech Syst Signal Process. https://doi.org/10.1016/j.ymssp.2022.109061
10. Jaeger M, Drichel P, Schröder M et al (2024) On magnetization deviations as the dominant cause for vibration harmonics in the spectrum of a PMSM drive. Archives of Electrical. Engineering https://doi.org/10.24425/aee.2021.137584
11. Craig RR, Bampton MC (1968) Coupling of Substructures for Dynamic Analyses. Aiaa J 6:1313
12. Klocke F, Brecher C (2017) Zahnrad- und Getriebetechnik: Auslegung – Herstellung – Untersuchung – Simulation. Carl Hanser, München
13. Hertz H (1882) Über die Berührung fester elastischer Körper. J Reine Angew Math: 156–171
14. Möllers W (1982) Parametererregte Schwingungen in einstufigen Zylinderradgetrieben: Einfluß von Verzahnungsabweichungen und Verzahn ungssteifigkeitsspektren. Diss. RWTH Aachen University
15. Kamper T, Flock S, Schelenz R (2016) Advanced load application on deformable ring gears in planetary gearboxes. Multibody Syst Dyn 36:323–337. https://doi.org/10.1007/s11044-015-9466-7
16. Fietkau P, Bertsche B (2013) Efficient Simulation of Gear Contacts Including Transient Elastohydrodynamic Effects. J Tribol. https://doi.org/10.1115/1.4024212
17. Ebrahimi S, Eberhard P (2006) Rigid-elastic modeling of meshing gear wheels in multibody systems. Multibody Syst Dyn 16:55–71. https://doi.org/10.1007/s11044-006-9021-7

18. Andersson A, Vedmar L (2003) A dynamic model to determine vibrations in involute helical gears. J Sound Vib 260:195–212. https://doi.org/10.1016/S0022-460X(02)00920-3
19. Wang J, Howard I (2004) The torsional stiffness of involute spur gears. Proceedings of the Institution of Mechanical Engineers, Part C. J Mech Eng Sci 218:131–142. https://doi.org/10.1243/095440604322787009
20. Meagher J, Wu X, Kong D et al (2011) A Comparison of Gear Mesh Stiffness Modeling Strategies. In: Proulx T (ed) Structural Dynamics, vol 3. Springer New York, New York, NY, pp 255–263
21. Weber C, Banaschek K (1955) Formänderung und Profilrücknahme bei gerad- und schrägverzahnten Rädern, 2nd edn. Vieweg, Braunschweig
22. Norm (2019) Calculation of load capacity of spur and helical gears: Part 1: Basic principles, introduction and general influence factors(6336 Teil 1)
23. Vedmar L, Andersson A (2003) A method to determine dynamic loads on spur gear teeth and on bearings. J Sound Vib 267:1065–1084. https://doi.org/10.1016/S0022-460X(03)00358-4
24. Liang X, Zhang H, Zuo MJ et al (2018) Three new models for evaluation of standard involute spur gear mesh stiffness. Mech Syst Signal Process 101:424–434. https://doi.org/10.1016/j.ymssp.2017.09.005
25. Brecher C (ed) (2023) FEM-Zahnkontaktanalyse STIRAK – Abschlussberichte: FVA Vorhaben 127 I–IX. FVA (Forschungsvereinigung Antriebstechnik e. V.)
26. Munro RG, Palmer D, Morrish L (2001) An experimental method to measure gear tooth stiffness throughout and beyond the path of contact. Proceedings of the Institution of Mechanical Engineers, Part C. J Mech Eng Sci 215:793–803. https://doi.org/10.1243/0954406011524153
27. Yesilyurt I, Gu F, Ball AD (2003) Gear tooth stiffness reduction measurement using modal analysis and its use in wear fault severity assessment of spur gears. Ndt E Int 36:357–372. https://doi.org/10.1016/S0963-8695(03)00011-2
28. Özgüven H, Houser DR (1988) Dynamic analysis of high speed gears by using loaded static transmission error. J Sound Vib 125:71–83. https://doi.org/10.1016/0022-460X(88)90416-6
29. Kubur M, Kahraman A, Zini DM et al (2004) Dynamic Analysis of a Multi-Shaft Helical Gear Transmission by Finite Elements: Model and Experiment. J Vib Acoust 126:398–406. https://doi.org/10.1115/1.1760561
30. Kahraman A (1993) Effect of axial vibrations on the dynamics of a helical gear pair. Vib Acoust (vibration Acoust 115:33–39
31. Parker RG, Vijayakar SM, Imajo T (2000) Non-Linear Dynamic Response of a Spur Gear Pair: Modelling and Experimental Comparisons. J Sound Vib 237:435–455. https://doi.org/10.1006/jsvi.2000.3067
32. Kim W, Yoo HH, Chung J (2010) Dynamic analysis for a pair of spur gears with translational motion due to bearing deformation. J Sound Vib 329:4409–4421. https://doi.org/10.1016/j.jsv.2010.04.026
33. Lei L (2010) A Multibody System Model for Meshing Gears. AMM 44–47:1273–1278. https://doi.org/10.4028/www.scientific.net/AMM.44-47.1273
34. Blockmans B, Tamarozzi T, Naets F et al (2015) A nonlinear parametric model reduction method for efficient gear contact simulations. Numerical Meth Engineering 102:1162–1191. https://doi.org/10.1002/nme.4831
35. Schulz C, Mulski S (2015) Modelling and Simulating Flexible Gears—A Solution-Oriented Approach
36. (2019) ISO 6336-3: Calculation of load capacity of spur and helical gears—Part 3: Calculation of tooth bending strength (6336-3)
37. Dassault Systemes Simulia Corp (2018) Simpack Documentation
38. Andary F, Berroth J, Jacobs G (2019) An Energy-Based Load Distribution Approach for the Application of Gear Mesh Stiffness on Elastic Bodies. J Mech Des. https://doi.org/10.1115/1.4043313
39. Andary F, Jacobs G, Trippe M et al (2020) Verzahnungsmodellierung für Systemsimulation – Abschlussbericht. FVA Vorhaben 764 I (Forschungsvereinigng Antriebstechnik e.V.)
40. GmbH SIMPACK (2020) Simpack Documentation. Firmenschr., SIMPACK GmbH (Release 2020)
41. Weber C, Banaschek K (1953) Formänderung und Profilrücknahme bei gerad- und schrägverzahnten Rädern. In: Fachgemeinschaft Getriebe, Antriebselemente (eds) Schriftenreihe Antriebstechnik. Friedr. Vieweg & Sohn, Braunschweig
42. Niemann G, Winter H (2003) Getriebe allgemein, Zahnradgetriebe – Grundlagen, Stirnradgetriebe: Band 2: Getriebe allgemein, Zahnradgetriebe – Grundlagen. Springer, Berlin (Stirnradgetriebe, 2., völlig neubearb. Aufl., 2. berichtigter Nachdr., korrigierter Nachdr. Maschinenelemente / G. Niemann H. Winter, Bd. 2.)
43. (2020) Rechnerischer Festigkeitsnachweis für Maschinenbauteile aus Stahl, Eisenguss- und Aluminiumwerkstoffen vol 7. VDMA Verlag, Frankfurt am Main (überarbeitete Auflage. FKM-Richtlinie)

Publisher's Note Springer Nature remains neutral with regard to jurisdictional claims in published maps and institutional affiliations.